Supporting Information

Surface Oxidation Layer-Mediated Conformal Carbon Coating on Si Nanoparticles for Enhanced Lithium Storage

Guangwu Hu,[a] Ruohan Yu,[a] Zhenhui Liu,[a] Qiang Yu,[a] Yuanyuan Zhang,[a] Qiang Chen,[a] Jinsong Wu,[a, b] Liang Zhou,[a] and Liqiang Mai[a]*

[a]State Key Laboratory of Advanced Technology for Materials Synthesis and Processing, Wuhan University of Technology, Wuhan 430070, China

[b]Nanostructure Research Centre (NRC), Wuhan University of Technology, Wuhan 430070, China

Email: liangzhou@whut.edu.cn (L. Zhou)

EXPERIMENTAL SECTION

Characterization. Scanning electron microscopy (SEM) and transmission electron microscopy (TEM) were performed on JEOL-7100F and JEM-2100F microscopes. High-angle annular dark field scanning transmission electron microscopy (HAADF-STEM) images and the energy dispersive X-ray spectroscopy (EDS) measurements were performed on a Talos F200S microscope. X-ray diffraction (XRD) patterns were collected using a Bruker D8 Advance X-ray diffractometer with a Cu Kα X-ray source. Raman spectra were recorded with a Renishaw INVIA Raman microscope. Thermo gravimetric analysis (TGA) was measured by a STA-449C apparatus. The surface areas were determined by a Tristar-3020 instrument. X-ray photoelectron spectroscopy (XPS) measurements were performed on a VG Multilab 2000 X-ray photoelectron spectrometer.

Electrochemical Measurement. To prepare the working electrodes, the active material, acetylene black, and sodium alginate were mixed in an agate mortar with a weight ratio of 7:2:1. The mixture was then grinded to form a homogeneous slurry and coated onto a Cu foil followed by drying. After being punched into discs, the working electrodes were obtained. The mass loading of active material was $1.0 - 1.5$ mg cm^{-2}. The working electrode and Li metal were used to assembled coin-type half cells (CR2016). The electrolyte was composed of 1.0 M LiPF$_6$ in a mixture of ethylene carbonate/dimethyl carbonate (1:1 in volume) with 10 vol.% fluoroethylene carbonate (FEC). Galvanostatic charge/discharge (GCD) measurements ($0.01 - 1.5$ V *vs.* Li$^+$/Li) were performed on a LAND CT2001A multichannel battery tester. Cyclic voltammetry (CV) was obtained on a PGSTAT302N Autolab potentiostat/galvanostat between 0.01 and 2.0 V at a scan rate of 0.1 mV s^{-1}. Electrochemical impedance spectra (EIS) were collected at a frequency range of 10 Hz to 100 kHz with a potential amplitude of 10 mV.

Si@SiO$_x$@C//LiFePO$_4$ and Si/C//LiFePO$_4$ full-cells were also assembled. The Si@SiO$_x$@C and Si/C was first cycled in half-cells for several cycles and then taken out in de-lithiated state for full-cell assembly. The cathodes were obtained by mixing LiFePO$_4$, super-P, and poly (vinylidenefluoride) (PVDF) with a mass ratio of 70:20:10, grinding, followed by coating onto an Al foil and drying. The cathode material/anode material weight ratio was around 6:1, and the full-cells were cycled in the voltage window of $2.4 - 3.8$ V at 0.2 C (1 C = 170 mA g^{-1}).
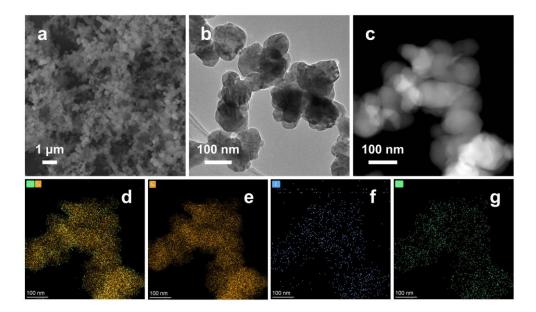
Figure S1. (a) SEM, (b) TEM, (c) HAADF-STEM image and the corresponding (d-g) EDS mappings of Si nanoparticles.
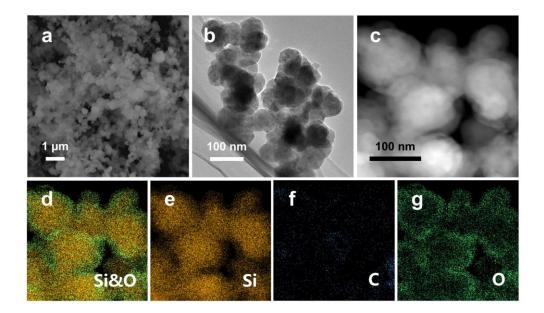

Figure S2. (a) SEM, (b) TEM, (c) HAADF-STEM image and the corresponding (d-g) EDS mappings of Si@SiO$_x$.
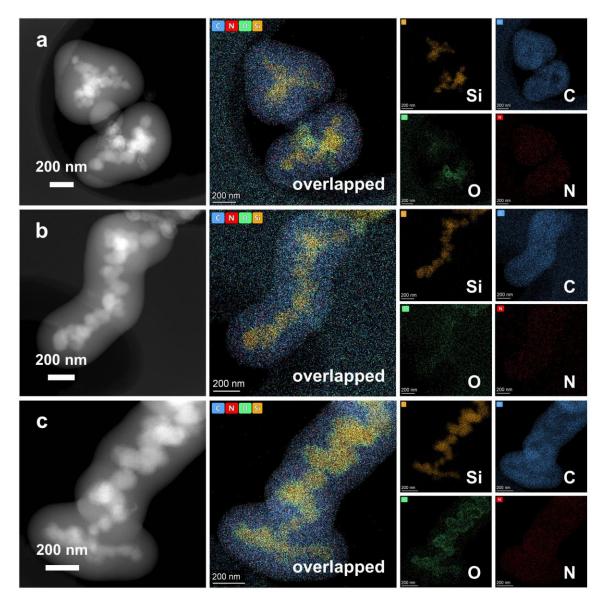
Figure S3. (a-c) HAADF-STEM images and their corresponding EDS mappings of Si@SiO$_x$@C on different particles.
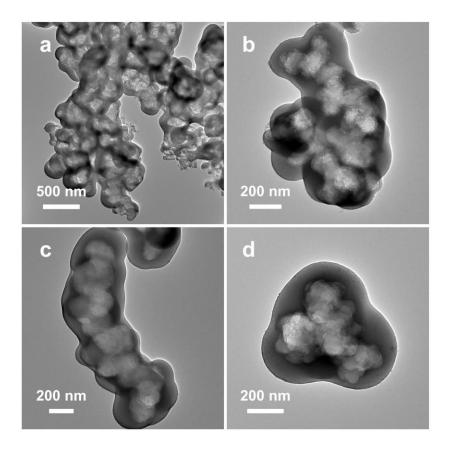
Figure S4. TEM images of the hollow carbon particles obtained by etching the Si@SiO$_x$@C with HF.
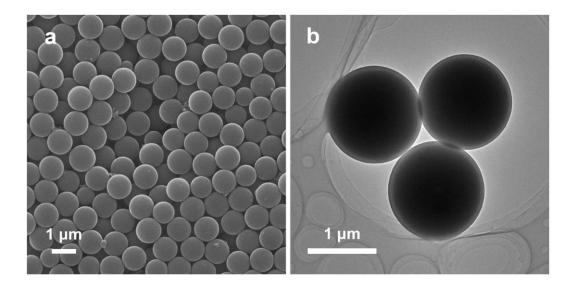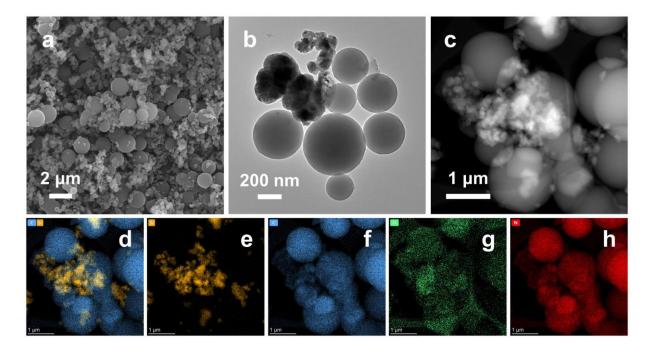

Figure S5. (a) SEM and (b) TEM image of CSs.

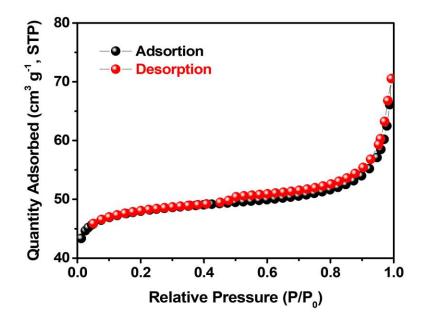**Figure S6.** (a) SEM, (b) TEM, (c) HAADF-STEM image and the corresponding (d-h) EDS mappings of Si/C.

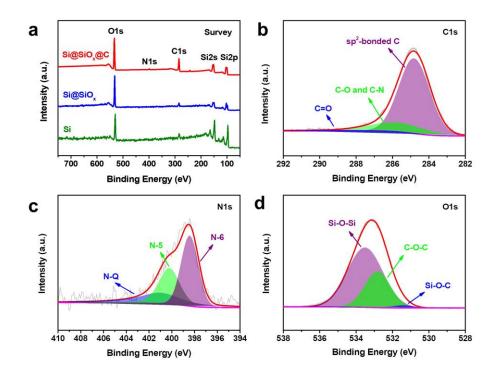**Figure S7.** N_2 adsorption/desorption isotherms of Si@SiO$_x$@C.

Figure S8. (a) XPS survey spectra of Si@SiO$_x$@C, Si@SiO$_x$ and Si; high-resolution (b) C1s, (c) N1s, and (d) O1s XPS spectra of Si@SiO$_x$@C.
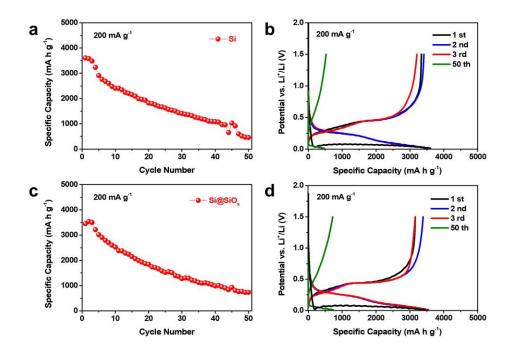
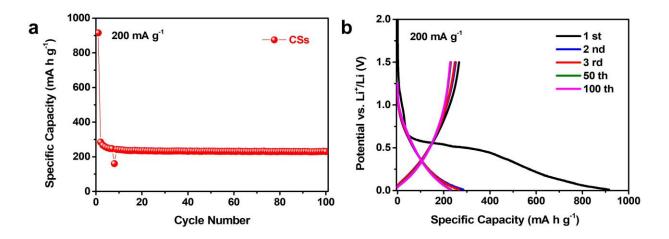**Figure S9.** Cycling performances and selected GCD profiles of (a, b) Si and (c, d) Si@SiO$_x$ at 200 mA g^{-1}.

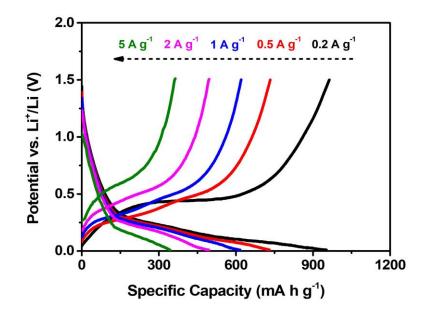**Figure S10.** (a) Cycling performance and (b) selected GCD profiles of CSs at 200 mA g^{-1}.

Figure S11. Charge-discharge curves of Si@SiO$_x$@C at various current densities.

Table S1. Lithium storage performances of various Si-based anode materials.

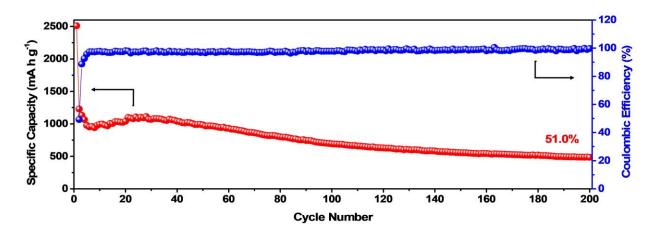| Ref.	Reversible Capacity (mAh g^{-1})	Initial Coulombic Efficiency (ICE)	Cycling Performance (mAh g^{-1})	Rate Capability (mAh g^{-1})	Electrochemical Window
This work	1168 (200 mA g^{-1})	64 %	94 % (500 mA g^{-1}, 500 cycles)	343 (5 A g^{-1})	0.01 – 1.5 V
[S1]	952 (200 mA g^{-1})	61 %	87 % (500 mA g^{-1}, 300 cycles)	406 (5 A g^{-1})	0.01 – 1.5 V
[S2]	620 (60 mA g^{-1})	89 %	75 % (300 mA g^{-1}, 500 cycles)	≈ 500 (3 A g^{-1})	0.005 – 1.0 V
[S3]	882 (50 mA g^{-1})	73 %	89 % (200 mA g^{-1}, 305 cycles)	466 (2 A g^{-1})	0.001 – 3.0 V
[S4]	964 (400 mA g^{-1})	≈ 59 %	92 % (400 mA g^{-1}, 100 cycles)	475 (3.2 A g^{-1})	0.01 – 1.5 V
[S5]	560 (100 mA g^{-1})	58 %	87 % (300 mA g^{-1}, 500 cycles)	230 (1.6 A g^{-1})	0.01 – 1.5 V
[S6]	1423 (100 mA g^{-1})	≈ 43 %	≈ 80 % (500 mA g^{-1}, 200 cycles)	586 (2 A g^{-1})	0.005 – 1.5 V
[S7]	895 (100 mA g^{-1})	73 %	103 % (1000 mA g^{-1}, 800 cycles)	≈ 250 (5 A g^{-1})	0.01 – 3.0 V
[S8]	1117 (50 mA g^{-1})	56 %	80 % (500 mA g^{-1}, 200 cycles)	≈ 500 (1 A g^{-1})	0.01 – 1.5 V

Figure S12. Cycling performance of Si@SiO$_x$@C sample with a lower carbon content at 500 mA g^{-1}.
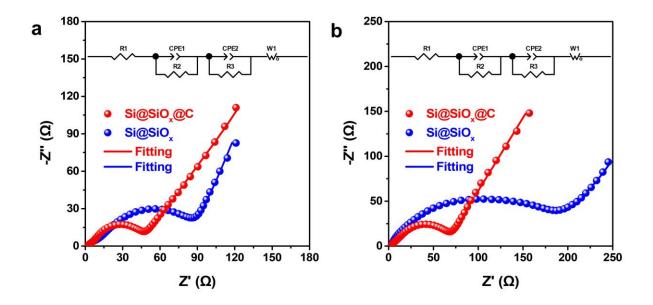

Figure S13. The electrochemical impedance spectroscopy plots of Si@SiO$_x$@C and Si@SiO$_x$ (a) before and (b) after cycling, the inset is equivalent circuit for fitting impedance plot.
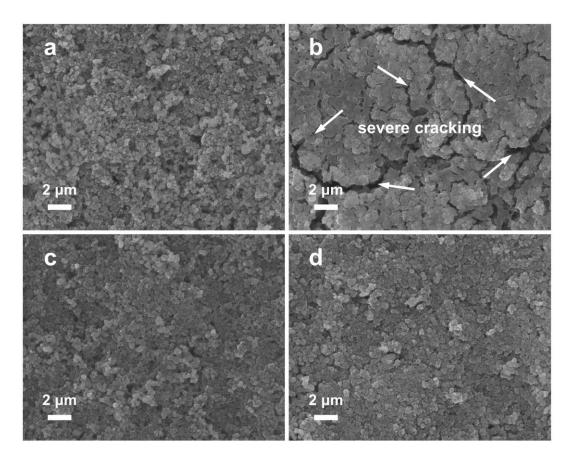
Figure S14. Top-view SEM images of Si@SiO$_x$ (a) before and (b) after 100 cycles at 200 mA g^{-1}, top-view SEM images of Si@SiO$_x$@C (c) before and (d) after 100 cycles at 200 mA g^{-1}.
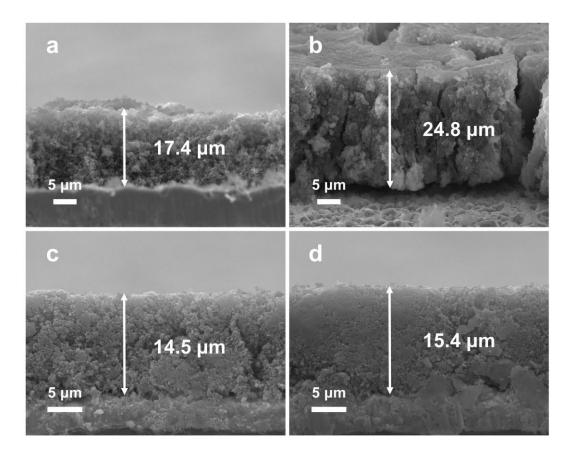
Figure S15. Cross-sectional SEM images of Si@SiO$_x$-based electrode (a) before and (b) after 100 cycles at 200 mA g^{-1}, cross-sectional SEM images of Si@SiO$_x$@C-based electrode (c) before and (d) after 100 cycles at 200 mA g^{-1}.
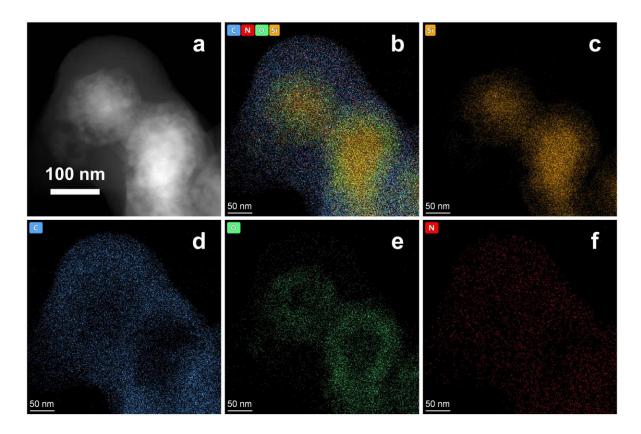
Figure S16. (a) HAADF-STEM image and the corresponding (b-f) EDS mappings of Si@SiO$_x$@C after 100 cycles at 200 mA g^{-1}.
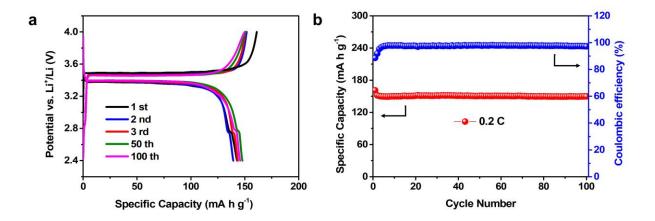

Figure S17. (a) Selected GCD profiles and (b) cycling performance of LiFePO$_4$ at 0.2 C.
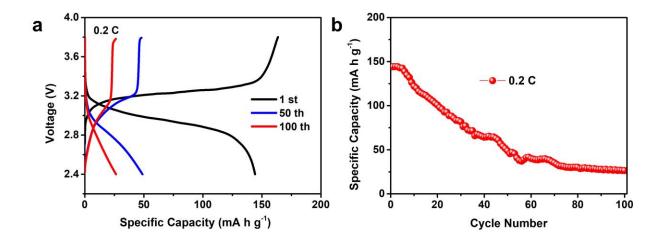
Figure S18. (a) Representative GCD profiles and (b) cycling performance of the Si/C//LiFePO$_4$ full-cell at 0.2 C.

References

[S1] Tian, H.; Tan, X.; Xin, F.; Wang, C.; Han, W. Micro-Sized Nano-Porous Si/C Anodes for Lithium Ion Batteries. *Nano Energy* **2015**, *11*, 490-499.

[S2] Xu, Q.; Li, J. Y.; Sun, J. K.; Yin, Y. X.; Wan, L. J.; Guo, Y. G. Watermelon-Inspired Si/C Microspheres with Hierarchical Buffer Structures for Densely Compacted Lithium-Ion Battery Anodes. *Adv. Energy Mater.* **2017**, *7*, No. 1601481.

[S3] Yang, T.; Tian, X.; Li, X.; Wang, K.; Liu, Z.; Guo, Q.; Song, Y. Double Core-Shell Si@C@SiO$_2$ for Anode Material of Lithium-Ion Batteries with Excellent Cycling Stability. *Chem-eur. J.* **2017**, *23*, 2165-2170.

[S4] Zhang, Y.; Du, N.; Zhu, S.; Chen, Y.; Lin, Y.; Wu, S.; Yang, D. Porous Silicon in Carbon Cages as High-Performance Lithium-Ion Battery Anode Materials. *Electrochim. Acta* **2017**, *252*, 438-445.

[S5] Liu, H.; Shan, Z.; Huang, W.; Wang, D.; Lin, Z.; Cao, Z.; Chen, P.; Meng, S.; Chen, L. Self-

Assembly of Silicon@Oxidized Mesocarbon Microbeads Encapsulated in Carbon as Anode Material for Lithium-Ion Batteries. *ACS Appl. Mater. Interfaces* **2018**, *10*, 4715-4725.

[S6] Kong, X.; Zheng, Y.; Wang, Y.; Liang, S.; Cao, G.; Pan, A. Necklace-Like Si@C Nanofibers as Robust Anode Materials for High Performance Lithium Ion Batteries. *Sci. Bull.* **2019**, *64*, 261-269.

[S7] Luo, H.; Wang, Q.; Wang, Y.; Xu, C.; Wang, B.; Wang, M.; Wu, H.; Zhang, Y. Nano-Silicon Embedded in MOFs-Derived Nitrogen-Doped Carbon/Cobalt/Carbon Nanotubes Hybrid Composite for Enhanced Lithium Ion Storage. *Appl. Surf. Sci.* **2020**, *529*, No. 147134.

[S8] Xie, C.; Xu, Q.; Sari, H. M. K.; Li, X. Elastic Buffer Structured Si/C Microsphere Anodes Via Polymerization-Induced Colloid Aggregation. *Chem. Commun.* **2020**, *56*, 6770-6773.